Lattice relaxation in the 1Bu state for the finite polyenes

BihYaw Jin and Robert Silbey

Citation: J. Chem. Phys. **102**, 4261 (1995); doi: 10.1063/1.469473
View online: http://dx.doi.org/10.1063/1.469473
View Table of Contents: http://jcp.aip.org/resource/1/JCPSA6/v102/i10
Published by the American Institute of Physics.

Lattice relaxation in the $1B_u$ state for the finite polyenes

Bih-Yaw Jin and Robert Silbey
Department of Chemistry and Center for Materials Science and Engineering, Massachusetts Institute of Technology, Cambridge, Massachusetts 02139

(Received 15 August 1994; accepted 2 December 1994)

The effect of electron correlation on the lattice relaxation of the lowest optically allowed $1B_u$ state of finite polyenes is investigated in this paper. We examine the competition between electron–electron interaction and electron-phonon coupling on the formation of localized lattice distortion in the $1B_u$ state for finite polyene with chain length up to 30 double bonds, using a number of theoretical models for the electron–electron interaction: short range Hubbard, extended Hubbard, and long-range Pariser–Parr–Pople models. The results show that in the intermediate to strong electron–electron interaction limit, the most stable geometry of the lowest optically accessible excitation is a self-trapped exciton (or a bipolaron), rather than separated solitons. © *1995 American Institute of Physics.*

I. INTRODUCTION

There has been extensive interests[1–4] in the study of conducting polymers in the recent years due to the observation of very high conductivities upon doping with strong electron acceptors or donors.[5] Polyacetylene and finite polyenes, consisting of alternating double and single bonds, are the simplest model systems for exploring various properties of one-dimensional conjugated systems.

In this paper, we study the lattice relaxation of the lowest optically allowed $1B_u$ state of finite polyenes. It is well known that in the Hückel approximation which neglect electron–electron (e-e) interaction, an electron-hole pair created upon photoexcitation of *trans*-$(CH)_x$ is unstable with respect to formation of a charged soliton-antisoliton (S^+S^-) pair.[6,7] This mechanism is an efficient way for charge separation and therefore possibly responsible for photoconductivity and photoinduced absorption associated with a charged soliton. Recently, the fast generation of a soliton-antisoliton pair (in the independent electron model) is suggested as the source of large optical nonlinearities[8] in polyacetylene, and the virtual soliton-antisoliton pair (instanton) formation enabled by the nonlinear zero-point fluctuations in the ground state is used to explain the large nonresonant nonlinear optical response.[9] Resonance Raman scattering (RRS) is known to be a good probe to the equilibrium geometry and dynamics of the resonant excited electronic state.[10,11] Hence, a large geometric change between ground and lowest $1B_u$ state due to soliton-antisoliton generation, as expected in the independent electron theory, should be reflected in the RRS as a broadband. The RRS study of finite polyenes with 3–13 double bonds made by Schaffer *et al.*[12] does not, however, show any indication of this effect. This suggests that electron–electron interaction may play an important role in the lattice relaxation of the $1B_u$ excited state. The purpose of this work is to examine whether the inclusion of electron correlation qualitatively changes the theoretical model of photogeneration of the soliton-antisoliton pairs through the $1B_u$ excited state.

Including electron–electron interaction perturbatively within the Su–Schrieffer–Heeger[1] (SSH)-extended Hubbard model in the continuum limit, Wu and Kivelson[13] have shown the formation of soliton-antisoliton pair in the $1B_u$ state persists. However, Grabowsky, Hone and Schrieffer[14] showed that the stable configuration in the $1B_u$ state is an exciton in a shallow well, unstable against thermal fluctuation at about 150 K. Hayden and Mele,[15] using a renormalization group method, have found that $1B_u$ state relaxes to a bound excitation, or an exciton.

We approach this problem by using standard methods of quantum chemistry. Since there are many excited configurations involved, it is necessary to include as many configurations as possible in order to obtain a correct description of the excited state. The effect of truncation of electron configurations is subtle. Including all configurations is difficult and becomes impossible as the size of the molecule increases. However, Schulten *et al.*[16] have shown that the $1B_u$ state consists mainly of single excitations. A direct diagonalization of the configuration interaction (CI) matrix within single excitation space for finite polyenes with chain lengths up to 40 double bonds is still feasible. By extrapolation from the experimental data for short chain polyenes, Schaffer *et al.*[12] have shown that the conjugation length for the polyene in the solid state limit is no longer than 40 double bonds. Therefore, the calculation carried out for a finite polyene can give useful information on the formation of lattice distortions in the solid state limit.

Using the intermediate exciton theory (i.e., a direct diagonalization of single excitation CI matrix in the exciton basis), Yaron and Silbey[17] have found that the lowest energy excited state for an undistorted polyene is an exciton state with the electron and hole tightly bound together (root mean square separation between electron and hole pair is about 2 unit cells). However, the photoexcited electron-hole pair in the $1B_u$ state of a polyene decays to a separated S^+S^- pair in the independent electron theory. Hence, the electron–electron interaction tends to keep the electron and hole together, while the electron-phonon coupling tends to separate the electron and hole and the associated lattice deformation. The interplay between the electron–electron interaction and electron-phonon coupling is therefore important for the formation of a localized distortion in the $1B_u$ excited state.

In this paper, we examine the lattice relaxation in the

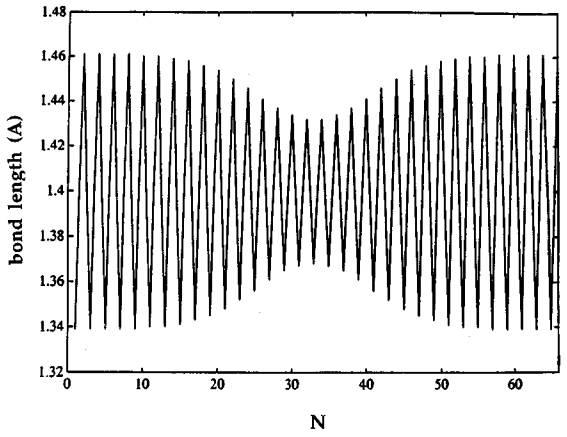

FIG. 1. A typical lattice configuration for the self-trapped exciton in the $1B_{1u}$ excited state within the PPP model. $N=66$, $\alpha=4.5$, $U=8$ eV, and $\epsilon=1$.

$1B_u$ state of finite polyenes ranging from $N=11$ to $N=35$, where N is number of unit cells (double bonds). The Hamiltonian matrix is diagonalized in a basis containing all single excitations from the restricted Hartree–Fock ground state. Minimization is performed by the simplex method without using derivative information. We have found several different local minima in different region of parameter space as a function of chain length. In the absence of electron–electron interaction, the lattice relaxes to charged soliton-antisoliton pair with a separation proportional to chain length. When the electron–electron interaction is present and the chain length is long enough, the soliton and antisoliton pairs are tightly bound in most of the parameter space. It is then more appropriate to call the excitation an electron-hole bipolaron or self-trapped exciton because it is a single entity (see Fig. 1). For short chains, in the limit of strong electron–electron interaction and strong electron-phonon coupling, the local minimum is a simple displacement along the $K=0$ (dimerization) mode. A localized distortion becomes favorable beyond a certain critical chain length which is a function of the strength of electron–electron and electron-phonon interactions.

II. THE MODEL

Assuming σ-π separation, the model Hamiltonian is a sum of two contributions: H_π and H_σ. σ electrons are modeled by simple additive potentials. In order to understand the effect of the range of force, electron correlation among π electrons is explicitly treated by three different models: a short range Hubbard, an extended Hubbard model, and a long range Pariser–Parr–Pople (PPP) model with different screening. In general, the Hamiltonian is given by

$$H_\pi=\sum_{nm\sigma} h_{nm}a^+_{n\sigma}a_{m\sigma}+\frac{1}{2}\sum_{m\sigma n\sigma'} \gamma_{nm}a^+_{n\sigma}a^+_{m\sigma'}a_{m\sigma'}a_{n\sigma}, \tag{1}$$

where $H_{nm}=\beta_{n,n\pm1}$ and 0 otherwise, the resonance integral β is assumed to be linear in bond length: $\beta(r)=t_0+\alpha(r-r_0)$ and α characterizes the strength of electron-phonon coupling. γ_{nm} is parametrized by Ohno's formula

$$\gamma_{nm}=\frac{U}{(1+U^2(\epsilon r_{nm}/e^2)^2)^{1/2}} \tag{2}$$

in the case of the PPP approximation and is given by $\gamma_{mn}=U\delta_{mn}$ and $\gamma_{mn}=U\delta_{nm}+V\delta_{mn\pm1}$ for the Hubbard and extended Hubbard models. In Eq. (2), ϵ is the dielectric constant, U denotes the onsite electron repulsion which is the difference between ionization potential and electron affinity of the atom. At large distance, γ has the Coulomb form $1/\epsilon r$. The Fock operator associated with the many body Hamiltonian, H_π, is given by

$$F=\sum_{mn\sigma} f_{nm}a^+_{n\sigma}a_{m\sigma} \tag{3}$$

with the matrix element

$$f_{nm}=h_{nm}+\sum_{n'} \gamma_{n'm}P_{n'n'}\delta_{nm}-\tfrac{1}{2}\gamma_{nm}P_{mn}, \tag{4}$$

where $P_{nm}=\Sigma_\sigma\langle a^+_{n\sigma}a_{m\sigma}\rangle$ is the single particle density matrix. The Fock matrix is diagonalized self-consistently,

$$F=\sum_{a\sigma} \epsilon_a c^+_{a\sigma}c_{a\sigma}+\sum_{r\sigma} \epsilon_r c^+_{r\sigma}c_{r\sigma}, \tag{5}$$

where $c^+_{a\sigma}$ creates one electron with spin σ in the best one electron molecular orbital ϕ_a. Ground and singly excited states can then be constructed from $|\text{vac}\rangle$,

$$|\Psi_0\rangle=\prod_{i\sigma}^{\text{occ}} c^+_{i\sigma}|\text{vac}\rangle, \tag{6}$$

$$|^1\Psi^r_a\rangle=(1/\sqrt{2})(c^+_{r\alpha}c_{a\beta}-c^+_{r\beta}c_{a\alpha})|\Psi_0\rangle. \tag{7}$$

The matrix elements between ground and singly excited states vanish from Brillouin's theorem. Matrix elements between two singly excited state are given by

$$\langle^1\Psi^r_a|H_\pi-E_0|^1\Psi^s_b\rangle=(\epsilon_r-\epsilon_a)\delta_{ab}\delta_{rs}-(rs|ba)+2(ra|bs). \tag{8}$$

Since the lowest optically allowed excitation is a $1B_u$ state, which consists mainly of singly excited configurations,[16] we expect that a diagonalization within the space spanned by all singly excited configurations should give a good description of this state. Furthermore, single CI is a size-consistent method,[18,19] so the results can be extrapolated to the large N limit.

In the presence of translational symmetry,[17] the single excitation CI matrix can be further reduced to block form in the exciton basis:

$$|\Psi_{\Delta K}\rangle=\frac{1}{\sqrt{N}}\sum_k e^{ik\Delta}|\Psi^{k+K}_k\rangle, \tag{9}$$

where Δ is the separation between electron and hole, K is the exciton momentum, and the molecular orbitals are character-

ized by the quasimomentum, k. Then the CI matrix can be diagonalized within each submatrix with fixed exciton momentum K, corresponding to exact diagonalization in the intermediate exciton theory. However, in the presence of lattice distortion, translational symmetry is broken and thus exciton momentum is no longer a good quantum number. We then have to diagonalize the whole singly excited CI matrix which is formidable since the size of this matrix is proportional to N^4. By restricting ourselves to the lattice distortions with mirror symmetry, and exploiting alternancy symmetry for the PPP model, the size of CI matrix can be reduced to about one fourth of the original. Once the localized distorted wavefunctions are found we can then restore translational symmetry by making a transformation to K space. This produces a band of distorted (''polaron'') states. However, if the effective mass of the distorted state is very large, then this does not alter the energy of the state. In this paper, we will assume that the effective mass is infinite, so a further transformation is unnecessary.

The σ-bond energy is approximated as a collection of harmonic oscillators. Thus, we obtain the total energy for the excited B_u state at a fixed nuclear configuration:

$$E_{\mathrm{tot}}(\mathbf{r}) = E_{\pi}(\mathbf{r}) + E_{\sigma}(\mathbf{r}), \tag{10}$$

where

$$E_{\sigma}(\mathbf{r}) = \tfrac{1}{2} K_{\sigma} \sum_{n} (r_n - r_0)^2, \tag{11}$$

r_0 is the equilibrium bond length in the absence of π-electron interaction and K_{σ} is the σ-bond spring constant.

In order to minimize chain end effects and facilitate the minimization in the absence of localized distortion, periodic boundary conditions are used throughout the calculation. In this case, the ground state is always doubly degenerate with respect to interchange of single and double bonds. Hence, cyclic chains always allow a soliton-antisoliton configuration, unlike open linear chain systems which do not have a degenerate ground state.[20]

The number of variables for the energy minimization in both ground and excited state are proportional to the size of polyene chain. Since it is impossible and unrealistic to do a direct N-dimensional minimization for large polyene, we restrict the energy minimization in some physically relevant subspace. We first optimize the geometry of the ground state along the only relevant coordinate: the dimerization mode. When we go to the $1B_u$ state, the single bonds acquire some double bond character and double bonds, single bond character. This is because a configuration with a single excitation replaces a bonding orbital by an antibonding orbital, hence the electron density is moved from double bonds to single bonds. As a result, bond alternation in the $1B_u$ state is weaker than in the ground state. As the chain length increases, the effect of excitation on the geometry become weaker, since the displacement along the dimerization mode goes like $N^{-1/2}$ as $N \to \infty$ if only delocalized relaxation along the dimerization mode is allowed. For this case, the potential surface for the excited state and ground state are exactly the same as $N \to \infty$. We have therefore restricted ourselves to the following four parameter space[20] which allows relaxation in the bond alternation and towards the soliton-antisoliton (S^+S^-) direction:

$$\begin{aligned} r_e(n) = r_g(n) - (-1)^n \delta_e + (-1)^n \frac{\phi}{2} \tanh\left(\frac{2R}{\xi}\right) \\ \times \left[\tanh\left(\frac{n - I_0 - R}{\xi}\right) + \tanh\left(\frac{n+1-I_0-R}{\xi}\right) \right. \\ \left. - \tanh\left(\frac{n-I_0+R}{\xi}\right) - \tanh\left(\frac{n+1-I_0+R}{\xi}\right) \right]. \end{aligned} \tag{12}$$

In Eq. (12) R denotes the separation between soliton and antisoliton pairs, ξ is the soliton width, ϕ represents the dimerization amplitude around S^+S^- configurations, and δ_e is the dimerization amplitude along the $K=0$ mode (i.e., the dimerization mode). Including minimization along $K=0$ is essential for the competition between formation of the localized bipolaron and simple displacement along the $K=0$ mode. We also define a dimensionless electron-phonon coupling constant $\lambda = 2\alpha^2/\pi K_{\sigma} t_0$.

Both the simplex and Powell direction set method[21] have been used for the minimization. However, the simplex method is usually faster than the latter. Hence, most of our calculations are carried out by simplex method. The procedure for the optimization is separated into the two steps: (1) For a given set of parameters, we minimize the total energy for the ground state along $K=0$ mode to get the equilibrium configuration $\mathbf{r}_g$ without using the empirical bond-order–bond-length (BOBL) relationship. (2) Starting from previous configuration, we minimize the excited state in the four-dimensional space (R, ξ, ϕ, δ_e).

The BOBL relationship is not used for minimization for the following two reason: (1) the σ-bond force constants depend on how the parameters in the BOBL relationship are chosen; (2) there is no analytical expression for this relation in the presence of electron–electron interaction, except for the Hubbard and extended Hubbard model. (In addition, Bredas *et al.*[22] have shown that BOBL and direct minimization in the excited state do not give the same result.) Hence, in order to get a consistent result, we have used the direct minimization for both the ground and excited states.

III. RESULTS AND DISCUSSIONS

A. Results in Hückel theory

In order to understand how the results in the presence of electron–electron interaction deviates from the independent electron theory, we briefly review some results for the Hückel model first. Table I shows lattice configurations at potential minimum of the $1B_u$ excited state in the Hückel limit for different N by setting the electron–electron interaction to zero.[23] In this limit, the perfect dimerized chain is always unstable with respect to the generation of a charged S^+S^- pair in the excited B_u state, and the binding energy is about 0.42 eV for chain length $N=50$. The lattice relaxation is qualitatively the same for all chain lengths in the Hückel limit. Since there is no electron correlation, no attraction exists between soliton and antisoliton pair except for the fi-

TABLE I. Chain length dependence for the sizes of charged soliton-antisoliton pairs in the $1B_u$ state for the Huckel model: $t_0=-2.5$ eV, $\alpha=6.47$ eV (Å), $K=53.3$ eV (Å)^2, and $\lambda=0.20$.

N	δ_g	E_{gap}	R	ξ	ϕ	E_b
26	0.057	1.69	6.27	4.10	0.050	−0.377
34	0.059	1.55	8.23	5.72	0.052	−0.413
42	0.059	1.47	10.25	6.73	0.051	−0.421
50	0.060	1.42	12.29	7.24	0.051	−0.419

nite size effect. The potential surface in the Hückel limit is shown in Fig. 2 with label $U=0$. One can see that the potential surface along R decreases very fast and starts to vary slowly when $R>2\xi$ and increase again when the S^+S^- pair meet from the other side of the ring. The separation between the S^+S^- pair at the potential minimum is about one-half of the chain length. Since the soliton is a domain wall between two bond alternated states, its binding energy relative to pure e^-h^+ state is determined by competition between two effects: (a) the tendency to increase the region of dimerized state and, hence, shrink the size of the undimerized soliton region and (b) the tendency to increase the domain wall such that the energy to put electrons in a small solitonic region is smaller due to the uncertainty principle. Table I also shows that the half width of the soliton increases as one increases the chain length ($\xi\sim7$ unit cells in the solid state limit). The transition from short polyene to polyacetylene for the lattice relaxation of the $1B_u$ excited state in the Hückel limit is smooth,[23] the electron-hole pair decays to a pair of charged solitons for all chain lengths.

B. Results in the PPP model

In Tables II and III, we show the results of minimization of total energy of $1B_u$ state for given N,t_0,U,K_σ, with different (α,ϵ) and (α,U) in the PPP model. Two different methods, which are on-site Coulomb repulsion U and dielectric constant ϵ respectively, have been used to parametrize the strength of the long range electron–electron interaction [see Eq. (2)].[24] We show how lattice relaxation in the excited $1B_u$ state depends on the the competition between electron-phonon and electron–electron interaction, i.e., the relative magnitude of α and U or ϵ. In the region with weak electron-phonon (small α) and strong electron–electron interaction (small ϵ or large U), there is no localized distortion, but a simple dimerization along the $K=0$ phonon mode at $N=34$. However, in the region with strong electron-phonon coupling (large α) and weak electron–electron interaction (strong ϵ or small U), the localized excitation is favored. Except in the absence of electron-electron interaction or very weak electron repulsion (ϵ very large or U very small), the soliton and antisoliton are tightly bound together to form a self-trapped exciton. From Tables II and III, we also find that the size of lattice distortion depends on the strength of the electron–electron interaction and the electron-phonon coupling. For a fixed α, the size of the lattice distortion decreases as the electron–electron interaction (U or ϵ) is increased. This is due to the attraction between the electron and hole becoming larger when the electron–electron interaction is increased through either U or ϵ. On the other hand, the localized lattice distortion becomes smaller when the electron-phonon coupling is increased at a fixed electron–electron interaction because a large distortion costs more elastic energy than a

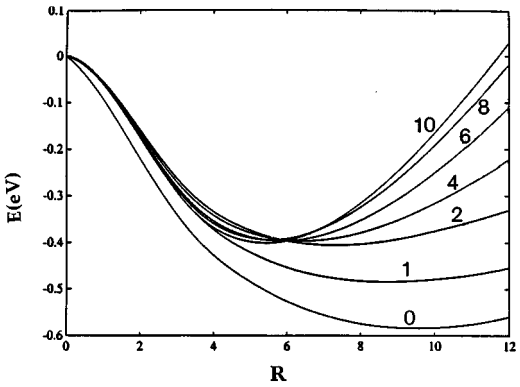

FIG. 2. The potential surfaces of $1B_{1u}$ states in the direction of the soliton-antisoliton separation, R, for different on-site electron repulsion ($U=0$–10) within the PPP approximation. $N=34$, $\alpha=6$, and $\epsilon=1$.

TABLE II. Relaxed configuration of polyene for different strength of electron–electron interaction, ϵ, and electron-phonon coupling, α: $N=34$; $K_\sigma=46.0$ eV (Å)^2.

ϵ	1.0	2.0	3.0	4.0	5.0	1.0	2.0	3.0	4.0	5.0
α			R					ξ		
4.0		7.22	8.26				5.00	2.66		
4.5		5.98	7.44	8.37	8.75		4.93	5.03	5.08	5.11
5.0	6.29	5.06	6.52	7.68	8.17	3.71	4.45	4.79	4.94	5.57
5.5	3.83	4.35	5.15	6.60	7.49	4.40	3.78	4.68	4.72	4.81
6.0	3.17	3.69	4.65	5.54	6.32	3.66	3.33	3.77	4.19	4.43
α			ϕ					δ		
4.0	0.0	0.018	−0.015	0.0	0.0	0.018	0.010	0.041	0.031	0.033
4.5	0.0	0.035	0.032	0.028	0.025	0.020	0.0031	0.0021	0.0022	0.003
5.0	0.018	0.047	0.042	0.037	0.036	0.0078	0.0	0.0	0.0	0.002
5.5	0.048	0.058	0.059	0.047	0.042	0.0022	0.0	0.0	0.0	0.0
6.0	0.064	0.072	0.065	0.058	0.053	0.0	0.0	0.0	0.0	0.0

TABLE III. Lattice relaxation in the $1B_u$ state for different strength of electron–electron interaction U and electron-phonon coupling α: $N=34$.

U	R	ξ	ϕ	δ_e
		$\alpha=4.75$		
0	8.2827	5.2638	0.0235	−0.0226
2			0.0	0.0256
4			0.0	0.0227
6			0.0	0.0219
8			0.0	0.0211
10			0.0	0.0206
		$\alpha=5.25$		
0	8.16	5.4951	0.0317	−0.0184
2			0.0	0.0324
4			0.0	0.0258
6			0.0	0.0238
8	6.33	3.23	0.018	0.0087
10	5.27	3.88	0.028	0.0046
		$\alpha=5.75$		
0	8.1969	5.2454	0.0419	0.0
2	6.9799	5.3448	0.0306	0.0057
4	6.3158	4.9860	0.0281	0.0072
6	5.6343	3.3869	0.0288	0.0059
8	4.2490	4.1917	0.0434	0.0025
10	3.6556	3.8655	0.0516	0.0015

small distortion does. This is similar to dependence of the size of soliton on the electron-phonon coupling in the polyacetylene with one soliton: the size of the soliton is inversely proportional to the electron-phonon coupling α in the continuum solid state limit without electron–electron interaction.

C. Potential energy surfaces

Figure 2 shows the potential surface of $1B_u$ state along the R direction for several different on-site electron repulsion values ($U=0$–10) in the PPP approximation. The potential surface for the Hückel limit, $U=0$, is almost flat when two soliton configurations are separated at opposite sides of the ring. A shallow well for the bound exciton is created by an increase of U from 0 to 1. The barrier for $U=1$ is due to the cyclic boundary imposed in the calculation. This suggests that the bound exciton is unstable with respective to thermal fluctuations if weak electron-electron interaction is used.[13] The lattice relaxation energy decreases as U is increased from 0 to around 2, and then starts to increase back to 0.3 eV again. We can also see the potential barrier for separating an electron-hole pair is much larger than thermal energy at room temperature. Note that an increase of on-site electron repulsion from $U=8$ to 10 is not as significant as an increase from $U=0$ to 2. Figure 3 shows the potential surface of the $1B_u$ state along the R direction for several different dielectric constants. In contrast with the (α,U) parametrization, there is a dramatic change in the relaxation energy along the R direction when going from $\epsilon=1$ to $\epsilon=2$. However, the change in the force constant is small in this limit. In the strong ϵ limit (Hubbard model), the potential surface becomes shallower which suggests that the effective interaction between S^+S^- is smaller. In both Figs. 2 and 3, the equilibrium separation become smaller as the electron–electron interaction is increased, consistent with the result obtained from minimization in the previous subsection. Figure 4 gives the typical behavior of $1B_u$ potential surfaces along the δ ($K=0$ mode) direction (delocalized distortion). Similar to the result from Hückel model, the lattice displacement along the δ direction decreases as N increases. The relative magnitude for the localized and delocalized distortion depends on the chain length. This point will be elaborated in the next subsection. The (R,ξ) contour plots for different U show that the potential surface for the R and ξ coordinates are almost decoupled and the force constants for the R are much smaller than ξ. The equilibrium position (R_0,ξ_0) moves toward the origin as U is increased, which implies that the attraction between soliton and antisoliton becomes stronger, as expected. We conclude that the dependence of potential well on the strength of electron–electron interaction and electron-phonon coupling is not small and an inclusion of electron–electron interaction produces a dramatic effect on the lattice distortion.

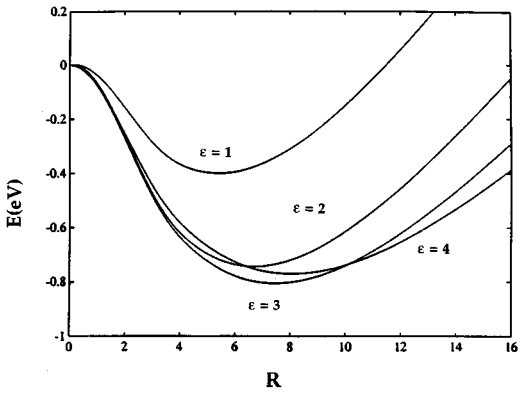

FIG. 3. The potential surfaces of $1B_{1u}$ states in the direction of the soliton-antisoliton separation, R, for different strength of electron–electron interaction parametrized by the dielectric constant e ($e=1$–4) within the PPP approximation: $N=50$; $\alpha=6$; $U=11.26$.

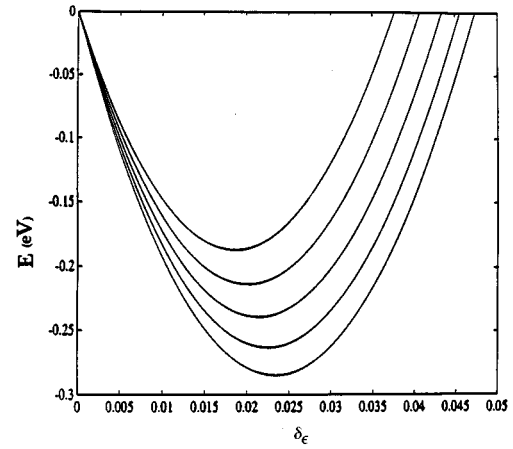

FIG. 4. The potential surfaces of $1B_{1u}$ states along the dimerization mode, $K=0$, within the PPP approximation. Five different electron-phonon couplings are used (from top to bottom: $\alpha=4$, 4.5, 5, 5.5, 6): $U=11.26$, $N=34$, and $\epsilon=1$.

TABLE IV. Chain length dependence of bipolaron formation: $t_0=-2.5$ eV; $\lambda=0.112$, $U=8.0$ eV; $\epsilon=1.0$; $K_\sigma=46.0$ eV (Å^2).

N	R	ξ	ϕ	δ
		$\alpha=4.5$		
22			0.0	0.0298
30			0.0	0.0228
38			0.0	0.0181
46			0.0	0.0147
54			0.0	0.0124
62			0.0	0.0107
66	7.73	7.55	0.019	0.0013
		$\alpha=4.75$		
22			0.0	0.0314
30			0.0	0.0239
38			0.0	0.0187
46			0.0	0.0153
50	7.73	2.22	0.0129	0.0059
54	6.69	6.62	0.0232	0.0018
58	8.14	4.48	0.0177	0.0020
62	6.31	6.95	0.0269	0.0008
		$\alpha=5.25$		
22			0.0	0.0346
26			0.0	0.0299
30			0.0	0.0257
34	6.33	3.23	0.0184	0.0087
38	5.44	5.15	0.0297	0.0033
42	5.07	5.41	0.0347	0.0018
46	6.19	3.98	0.0261	0.0024
50	5.34	5.13	0.0331	0.0013
54	5.28	5.19	0.0341	0.0008

D. Chain length dependence

Table IV shows the chain length dependence of the bipolaron formation. Note that the onset of the instability with respect to a local polaronlike excitation depends on the relative strength of electron-phonon and electron–electron interaction. We choose $U=8$ and $\lambda=0.112$ in Table IV. The size of localized distortion is small (typically around or less than 7 unit cells) as shown in Fig. 1, Tables II, and III. Table V shows that the onset of localized polaronic excitation in the $1B_u$ state depends on chain length. For a given electron–electron and electron-phonon coupling, there is a corresponding localization length $L_p(U,\alpha)$ such that no localized distortion is favored when the chain length $L_N<L_p$ and the minimum is just a simple distortion along the $K=0$ mode. In the solid state limit, the local minimum along the $K=0$ mode become less stable with respect to the bipolaron formation in parameter space (α,U) or (α,ϵ). This is reminiscent of the result of Longuet-Higgins and Salem[25] on the onset of dimerization for finite polyene in the ground state as a function of N. Longuet-Higgins and Salem show that there is no bond alternation for short polyene when $N=4n+2<N_{\text{critical}}$ (aromaticity), but the alternated polyene becomes energetically favorable when $N>N_{\text{critical}}$ due the gain in the elastic energy compared to the small loss of electronic energy around Fermi surface. However, the geometry of the $1B_u$ excited state has more instabilities than in the ground state. Besides the instability along $K=0$ modes, the directions with localized bipolaron or bisoliton formation are also important. Similar to Longuet-Higgins and Salem's result for the ground state, a delocalized distortion along $K=0$ mode becomes less stable than a localized distortion when N is larger than N_{critical}. If we assume that the localized distortion cannot move (all calculations performed in this paper have made this approximation), we find by extrapolation from Table IV that the delocalized distortion is always unstable with respect to the formation of a localized distortion in the solid state limit.[26–29]

TABLE V. Critical chain length for the formation of bipolaron. Parameters are the same as in Table IV.

α	N_p
4.5	66
4.75	50
5.25	34

TABLE VI. Dependence of bipolaron formation on the force range for $N=42$, $\alpha=6.0$ eV/Å. This figure shows the effect of force range by three different models: Hubbard, extended Hubbard, and the PPP model.

						Ground state		Excited state	
U	V	R	ξ	ϕ	δ	C–C	C=C	C–C	C=C
				Hubbard model					
0	0	10.2	6.15	0.0490	0.0036	1.45	1.35		
2	0	10.1	6.69	0.0488	0.0044	1.45	1.35		
4	0	10.0	7.21	0.0488	0.0055	1.45	1.35		
6	0	9.84	7.69	0.0489	0.0069	1.45	1.35		
8	0	9.51	8.29	0.0480	0.0198	1.45	1.35		
10	0	8.49	8.62	0.0471	0.0319	1.45	1.35		
				Extended Hubbard model					
8	1	8.75	6.37	0.045	0.0	1.46	1.34		
8	2	6.60	5.40	0.052	0.0	1.47	1.33		
8	4	3.85	4.47	0.050	0.0	1.49	1.31		
8	6			0.00	0.011	1.49	1.31	1.48	1.32
8	8			0.00	0.0092	1.50	1.30	1.49	1.31
				PPP model					
0		10.21	6.15	0.0490	0.0036	1.45	1.35		
2		6.35	5.95	0.0417	0.0019	1.46	1.34		
4		5.76	4.53	0.0380	0.0022	1.47	1.33		
6		5.12	3.16	0.0373	0.0023	1.49	1.31		
8		3.51	4.03	0.0590	0.0006	1.50	1.30		
10		3.49	3.43	0.0562	0.0006	1.51	1.30		

E. Effect of range of the interaction

In Sec. III B we have already used the dielectric constant, ϵ, and on-site electron–electron repulsion, U, to scale the the range and strength of the electron–electron interaction. In this subsection, we will study the effect of force range by concentrating on three commonly used models: Hubbard, extended Hubbard, and PPP model, and their effect on the the bipolaron formation. The results are shown in the Table VI. Since on-site electron–electron interaction in the Hubbard model cannot create an effective attraction between electron and hole pair, the interaction between soliton and antisoliton pair is smaller than in PPP. The optimized ground state geometry for the Hubbard model shown in Table VI is the same as that in the Hückel model, and the relaxed geometry in the $1B_u$ state is a separated S^+S^- pair

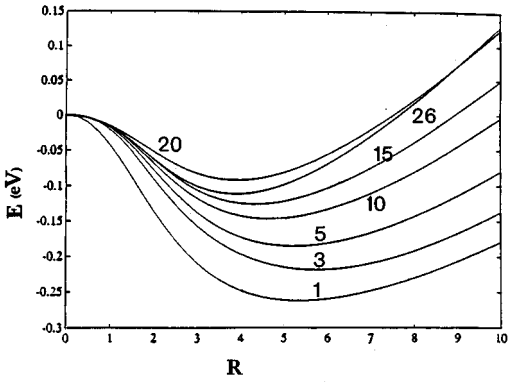

FIG. 5. The effect of the number of configurations on the potential surfaces within the extended Hubbard model. The single excitation configurations are selected from amongst the $2n$ innermost self-consistent field molecular orbitals, where n is given in the figure: $N=42$, $\alpha=6$, $U=8$, and $V=4$.

due to the lack of effective interaction between electron and hole associated with soliton and antisoliton configuration. Table VI shows that there is only a small change in the excited state geometry in the presence of U. The separation, R, decreases slightly as U is increased.

Both the extended Hubbard model and the PPP model give strong modifications of the geometric relaxation in the $1B_u$ excited state with respective to the Hückel model. The interatomic Coulomb interaction is necessary for the formation of an exciton and, therefore, is also important for the formation of the bound soliton-antisoliton pairs (self-trapped exciton). As shown in Table VI, the interaction between a soliton and antisoliton pair becomes stronger as V/U is increased for $N=42$. When V/U is larger than $\frac{1}{2}$, the energy of a localized self-trapped state becomes higher than a delocalized distortion along the $K=0$ mode. This transition is not observed for the PPP model in the Table VI. However, as we have shown earlier, the same kind of transition does occur in the PPP model when the chain length is long enough. From Table VI, we find that even the short range interaction of the extended Hubbard model can produce significant electron-hole attraction within the single excitation CI level so as to produce a tightly bound charged S^+S^- pair.

F. Effect of number of configurations

In Fig. 5, we show the effect of the strength of electron correlation (by increasing the number of electron configurations taken into account) on the potential surface along R direction. The number of electron configurations is another way to measure the strength of electron correlation. From Fig. 5 one can see that if only a few states are used for configuration interaction, the potential relaxes deeply into the band gap and is shallower relative to far separated S^+S^- pairs. When more configurations are taken into account, the equilibrium separation becomes smaller and the barrier to separated S^+S^- higher. This suggests that the results of Grabowski *et al.*,[14] the potential barrier for separating S^+S^- is about 150 K in the $N=\infty$ limit, might be seriously in error due to their including only one spin adapted configuration in their calculation.

IV. CONCLUSIONS

In this paper, we have performed minimization for both ground and excited states by single excitation CI on cyclic polyenes with chain lengths up to 35 double bonds. When we restrict minimization to the dimerization mode, the general behavior of a finite polyene going from ground state to the $1B_u$ excited state is that the single bonds acquire double-bond character and double bonds, single-bond character, with and without inclusion of electron correlation. In the solid state limit for this case, no change in the potential surface can be induced by exciting one electron to the $1B_u$ excited state. However, this can still produce subtle effects in the resonance Raman scattering.[30]

The competition between electron–electron interaction and electron-phonon coupling gives rise to more complicated localized lattice distortion when we perform the minimization in the four-dimensional soliton-antisoliton subspace. Depending on the chain length and relative strength of electron–electron interaction and electron-phonon coupling, a simple change of dimerization amplitude, a self-trapped exciton or a separated soliton-antisoliton pair may become the most stable state in the $1B_u$ excited state. However, if the chain length is long enough, a localized polaronlike excitation is always energetically favored. In the intermediate and strong electron–electron interaction limit, we find that the lowest optically accessible excited state relaxes to a self-trapped exciton state instead of soliton-antisoliton configuration. Hence, in this case a photogenerated current cannot be induced through the lowest B_u state because a self-trapped exciton cannot carry photocurrent. However, higher lying band states can decay to charged S^+S^- pairs, which are the charge carriers observed in many experiments. Note, however, that the calculation performed here, based on adiabatic approximation, is not valid for band states, due to the numerous level crossings in the band states. Since the coupling between the π electrons and σ core is very strong, the charged S^+S^- pair must be described nonadiabatically.

Due to the ability to study ordered single crystal, of polydiacetylene, its lowest excited state has been unambiguously identified as an exciton state. PDA-PTS shows excitonic absorption near 2 eV while the threshold for photoconductivity is at 2.5 eV because extra kinetic energy is required to achieve charge separation. When interacting with a phonon coordinate, this exciton relaxes to a self-trapped state. However in *trans*-$(CH)_x$, the energy gaps between exciton and band states are small compared to inhomogeneity of *trans*-$(CH)_x$ samples used in most experiments, therefore it is difficult to distinguish the onset of optical transition and photoinduced current in the *trans*-$(CH)_x$ as was done in the case of polydiacetylene. Thus the question of the nature of the optically absorbing state (exciton vs band) in polyacetylene is difficult to determine.

It would be interesting to look at the dynamical properties of the self-trapped exciton in the excited $1B_u$ state in the presence of electron correlation.[6] We can then get information for the coupling of self-trapped exciton between different sites and the time scale of the self-trapped exciton to be formed in a photoexcitation processes, which are completely

neglected in the this paper. Further work along this direction is in progress.

ACKNOWLEDGMENTS

We thank Dr. Yaron for useful discussions. The research was sponsored by the National Science Foundation (NSF).

[1] W. P. Su, J. R. Schrieffer, and A. J. Heeger, Phys. Rev. B **22**, 2099 (1980).
[2] D. Baeriswyl, in *Theoretical Aspects of Band Structure and Electronic Properties of Pseudo-One-Dimensional Solids*, edited by H. Kamimura (Reidel, Dordrecht, 1985), pp. 1–48.
[3] A. J. Heeger, S. Kivelson, J. R. Schrieffer, and W.-P. Su, Rev. Mod. Phys. **60**, 781 (1988).
[4] D. Baeriswyl, D. K. Campbell, and S. Mazumdar, *Conjugated Conducting Polymers* (Berlin, New York, 1992).
[5] C. K. Chiang, C. R. Fincher, Y. W. Park, A. J. Heeger, H. Shirakawa, E. J. Louis, S. Gau, and A. G. MacDiarmid, Rhys. Rev. Lett. **39**, 1098 (1977).
[6] W. P. Su and J. R. Schrieffer, Proc. Natl. Acad. Sci. USA, **77**(10), 5626 (1980).
[7] R. Ball, W. P. Su, and J. R. Schrieffer, J. Phys. Paris Colloq. **44**, C3-429 (1983).
[8] T. W. Hagler and A. J. Heeger, Chem. Phys. Lett. **189**, 333 (1992).
[9] M. Sinclair, D. Moses, K. Akagi, and A. J. Heeger, Phys. Rev. B **38**, 10 724 (1988).
[10] J. Tang and A. C. Albrecht, in *Raman Spectroscopy: Theory and Practics*, edited by H. A. Szymanski (Plenum, New York, 1970), pp. 33–68.
[11] Anne B. Myers and Richard A. Mathies, *Biological Applications of Raman Spectroscopy*, edited by T. Spiro (Wiley, New York, 1987).
[12] H. E. Schaffer, R. R. Chance, K. Knoll R. J. Silbey, and R. R. Schrock, J. Chem. Phys. **94**, 4161 (1992).
[13] W.-K. Wu and S. Kivelson, Phys. Rev. B **34**, 3523 (1986).
[14] M. Grabowski, D. Hone, and J. R. Schrieffer, Phys. Rev. B **31**, 7850 (1985).
[15] G. W. Hayden and E. J. Mele, Phys. Rev. B **34**, 5484 (1986).
[16] K. Shulten, I. Ohmine, and M. Karplus, J. Chem. Phys. **64**, 4422 (1976).
[17] D. Yaron and R. Silbey, Phys. Rev. B **45**(20), 1655 (1992).
[18] W. Meyer, Int. J. Quantum Chemistry, **5**, 341 (1971).
[19] W. Meyer, J. Chem. Phys. **58**, 1017 (1973).
[20] Z. Shuai and J. L. Bredas, J. Chem. Phys. **97**, 5970 (1992).
[21] W. H. Press, B. P. Flannery, S. A. Teukolsky, and W. T. Vetterling, *Numerical Recipes: The Art of Scientific Computing* 1st Ed. (Cambridge University Press, New York, 1986).
[22] J. L. Bredas and J. M. Toussaint, J. Chem. Phys. **92**, 2624 (1990).
[23] J. L. Bredas and A. J. Heeger, Chem. Phys. Lett. **154**, 56 (1989).
[24] Note that the two different parametrization of the electron–electron interaction do not give exactly the same qualitative trend as a function of scaling in U and ϵ for many properties, such as the potential surface which we will show later. In the U parametrization, the Hückel limit is recovered by setting $U=0$, while electron–electron interaction always exists in the ϵ parametrization. We get the Hubbard model as $\epsilon\rightarrow\infty$ since the on-site electron repulsion is U for all ϵ.
[25] H. C. Longuet-Higgins and L. Salem, Proc. R. Soc. London, Ser. A **251**, 172 (1959).
[26] As pointed out by Shuai *et al.* (Ref. 20) the Huang-Rhys factor, defined by $S=\Sigma_s(\omega_0/2\hbar)(\Delta_{js}-\Delta_{is})^2$, tends to decrease first with the increasing of the chain length but starts to increase after some critical length in the Huckel model, which has been been used to explain the photoabsorption experiments on short polyenes (Ref. 27) and β-carotene (Ref. 28). In the presence of electron correlation, the same experimental results can be qualitatively explained by the chain length dependence of the bipolaron formation discussed here (Ref. 29). However, the calculation performed here is for polyene chains with periodic boundary condition, further calculation for the open chains need to be performed.
[27] M. F. Grainville, B. E. Kohler, and J. B. Snow, J. Chem. Phys. **75**, 3765 (1981).
[28] A. R. Mantini, M. P. Marzocchi, and G. Smulevich. J. Chem. Phys. **91**, 85 (1989).
[29] Z. Shuai, private communication.
[30] B. Y. Jin and R. Silbey, preceding paper, J. Chem. Phys. **102**, 4251 (1995).